PROGRESS IN PHOTOVOLTAICS: RESEARCH AND APPLICATIONS
Prog. Photovolt: Res. Appl. (2012)
Published online in Wiley Online Library (wileyonlinelibrary.com). DOI: 10.1002/pip.2263

RESEARCH ARTICLE

A novel analytical model for determining the maximum power point of thin film photovoltaic module

Joe-Air Jiang*, Yu-Ting Liang, Jen-Cheng Wang, Yu-Li Su, Kun-Chang Kuo and Jyh-Cherng Shieh

Department of Bio-Industrial Mechatronics Engineering, National Taiwan University, No. 1, Sec. 4, Roosevelt Road, Taipei 10617, Taiwan

ABSTRACT

Achieving the maximum power output from photovoltaic (PV) modules is indispensable for the operation of grid-connected PV power systems under varied atmospheric conditions. In recent years, the study of PV energy for different applications has attracted more and more attention because solar energy is clean and renewable. We propose an efficient direct-prediction method to enhance the utilization efficiency of thin film PV modules by tackling the problem of tracking time and overcoming the difficulty of calculation. The proposed method is based on the p–n junction recombination mechanism and can be applied to all kinds of PV modules. Its performance is not influenced by weather conditions such as illumination or temperature. The experimental results show that the proposed method provides high-accuracy estimation of the maximum power point (MPP) for thin film PV modules with an average error of 1.68% and 1.65% under various irradiation intensities and temperatures, respectively. The experimental results confirm that the proposed method can simply and accurately estimate the MPP for thin film PV modules under various irradiation intensities and temperatures. In future, the proposed method will be used to shed light on the optimization of the MPP tracking control model in PV systems. Copyright © 2012 John Wiley & Sons, Ltd.

KEYWORDS

direct-prediction method; maximum power point (MPP); photovoltaic (PV) modules; thin film

***Correspondence**

Joe-Air Jiang, Department of Bio-Industrial Mechatronics Engineering, National Taiwan University, No. 1, Sec. 4, Roosevelt Road, Taipei 10617, Taiwan.
E-mail: jajiang@ntu.edu.tw

Received 18 January 2012; Revised 23 April 2012; Accepted 28 May 2012

1. INTRODUCTION

Nowadays, the study of photovoltaic (PV) energy for various applications has entered the spotlight because of the shortage of nonrenewable energy resources such as coal, petroleum, and natural gas [1]. Not only are these resources limited but their use has already led to serious problems with environmental pollution [1]. People are looking for new sources of energy to add to or replace traditional ones. For these reasons, many nations are already seeking new alternative sources of energy and have invested much money in related research and development [2]. The need for energy-efficient electrical power sources in remote locations has been another driving force behind research endeavors to develop integrated energy systems. In particular, advancements in wind and PV generation technologies have been applied to develop wind-alone [3], PV-alone [4–6], grid-connected PV [7–9], and hybrid wind/PV configurations [10–12]. The use of PV modules has already allowed solar energy to become a clean reliable source of renewable energy [13] that many feel can efficiently mitigate the worst effects of global warming [14–16].

There are many kinds of PV modules, but silicon is the most common material used in their fabrication because of its better conversion efficiency [17]. Nevertheless, given their high price and difficulty of processing, PV modules made from silicon may not be a viable alternative to completely replace traditional power generation methods. Thin film solar cells, by contrast, can be viewed as an important alternative [18]. The advantages of using thin film PV modules are that they have a wide receiving spectra, are unaffected by temperature, and have low costs. Consequently, the development of thin film PV modules has become a priority these days.

The methods of enhancing the utilization efficiency involve not only changes in material [19] but also

maximum power point tracking (MPPT) [20]. A PV module has a nonlinear characteristic caused by a change in atmospheric conditions. MPPT methods are used to seek the maximum power of the PV module [21]. Generally, the commonly used methods to track the maximum power point (MPP) are the perturbation and observation [22–24], incremental conductance methods [25,26], fuzzy logic controllers [27,28], and other methods [29]. Being simple of operation and easy to understand, the perturbation and observation methods are often used. The load can be increased or decreased periodically, but some energy loss is inevitable near the MPP. The main electrical parameters of the solar cell are a function of the resistance, which can result in low energy-conversion efficiency in the PV modules [30–33] and a deterioration of the maximum power with varying resistance values [30,34]. The corresponding open-circuit voltages (V_{oc}) and short-circuit currents (I_{sc}) of a single solar cell are both affected by such variations in resistance [30,34]. Furthermore, there is a substantial decrease in the fill factor and dramatic variation in the MPP in a single solar cell with a change in the resistance [34]. The experimental results also demonstrate that the resistance has a critical effect on the characteristics of PV modules. Therefore, we must take the effect of the resistance into consideration in order to accurately evaluate the characteristics of PV modules from a single irradiated *I–V* characteristic curve.

In summary, this study focuses on the resistance effect in solar cells. A new and simple method is proposed to directly determine the MPP of thin film PV modules from one point on an irradiated current–voltage characteristic curve. This direct-prediction method can be used to enhance the utilization efficiency of thin film PV modules. Our method can track the MPP in real time to avoid the problem of energy loss. Moreover, this estimation method can also be applied to all kinds of PV modules and bring great benefits to the photovoltaic industry as a whole.

The rest of this paper is organized as follows. Section 2 explains the theoretical basis of the proposed prediction method for thin film PV modules, which is based on the p–n junction recombination mechanism in a semiconductor. Section 3 describes the experimental process used to verify the performance of the proposed method. Section 4 is divided into two parts. The first one discusses the basic performance evaluation of thin film PV modules with different numbers of series-connected (N_S) and parallel-connected (N_P) cells (or sub-modules), and the second examines the performance of thin film PV modules under various irradiation intensities and temperatures. Conclusions are given in Section 5.

2. THEORETICAL BASIS OF THE PROPOSED METHOD

The irradiation behaviors of PV modules are known to be nonlinear, but there exists one operating point where they generate maximum power. However, the nonlinearity means that the MPP of PV modules cannot be tracked quickly and accurately using traditional methods. Fortunately, the nonlinear irradiation behaviors of thin film PV modules can be understood using the p–n junction recombination mechanism of semiconductors. In this study, we propose a simplified method to directly estimate the MPP using the p–n junction theory so as to allow the thin film PV module to achieve maximum utilization efficiency.

The equivalent circuit of thin film PV modules based on the p–n junction theory is shown in Figure 1, where I_g is the photocurrent (A); R_{sh} is the parallel resistance (ohm), and R_s is the series resistance (ohm), which includes excessive contact resistance. Both R_s and R_{sh} are influenced by various conditions, such as varying illumination intensity levels and temperatures [31,32]. Most commonly, PV modules are composed of a number of either series-connected or parallel-connected cells. Therefore, the thin film PV modules can be assumed to be composed of a number of cells connected in series (N_S) or parallel (N_P). Thus, we impose additional modifying terms (N_S and N_P) in the proposed model where N_S and N_P represent the number of series-connected and parallel-connected cells in the thin film PV modules, respectively. By following the conventions in [33], the output current I of the thin film PV module is given by the following equation using the symbols shown in Figure 1:

$$I = I_g - I_d - V_d/R_{sh} \tag{1}$$

where I_d and V_d are the current and voltage of the diode. The V_d is given by

$$V_d = V + IR_s \tag{2}$$

and the current I_d can also be expressed by

$$I_d = I_{sat}\left\{\exp\left[\frac{qV_d}{nN_S kT}\right] - 1\right\} \tag{3}$$

The ideality factor (n) is usually set as "1" when only the

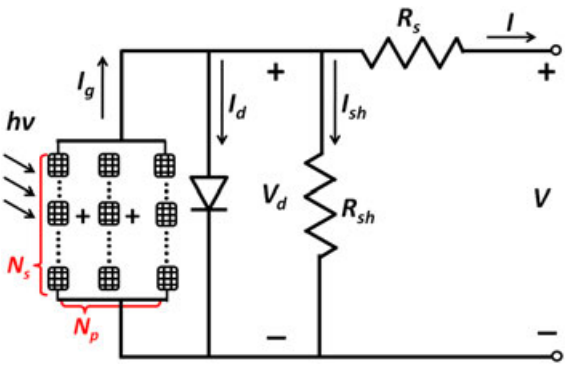

Figure 1. A diagram of the equivalent circuit for thin film PV modules.

diffusion current flows across the junction and "2" when the recombination current dominates [33]. Therefore, we always consider the ideality factor as a constant. I_{sat} is the reverse saturation current of the PV modules (A). The terms related to the parallel resistance R_{sh} can be generally ignored, because the parallel resistance of thin film PV modules is relatively high in the majority of practical cases. When thin film PV modules are connected to the load, the circuit parameters (I and V) in Eqs (1) and (2) are changed to I_{pv} and V_{pv}, respectively. Consequently, the output current of the thin film PV modules (I_{pv}) can be expressed by

$$I_{pv} = I_g - N_P I_{sat}\left\{ \exp\left[\frac{q\left(V_{pv} + I_{pv}R_s\right)}{nN_S kT}\right] - 1\right\} \quad (4)$$

The generated power of thin film PV modules is

$$P_{pv} = I_{pv}V_{pv} \quad (5)$$

and the power slope β with respect to the voltage variation of PV modules can be expressed as

$$\beta = \frac{dP_{pv}}{dV_{pv}} = I_{pv} + \frac{dI_{pv}}{dV_{pv}}V_{pv} \quad (6)$$

We can substitute Eq. (4) into Eq. (6) and then obtain the power slope β as follows:

$$\begin{aligned}\beta = {} & I_g - N_P I_{sat}\left\{ \exp\left[\frac{q\left(V_{pv} + I_{pv}R_s\right)}{nN_S kT}\right] - 1\right\} \\ & -N_P I_{sat}V_{pv}\frac{q}{nN_S kT}\exp\left[\frac{q\left(V_{pv} + I_{pv}R_s\right)}{nN_S kT}\right]\left(1 + \frac{dI_{pv}}{dV_{pv}}R_s\right)\end{aligned} \quad (7)$$

When the thin film PV modules operate at their MPP, the power slope $\beta = 0$. Eq. (7) can be further simplified to

$$\begin{aligned}\frac{I_g + N_P I_{sat}}{N_P I_{sat}} = {} & \exp\left[\frac{q\left(V_{mp} + I_{mp}R_s\right)}{nN_S kT}\right] \\ & \left\{1 + \frac{qV_{mp}}{nN_S kT} + \frac{qV_{mp}R_s}{nN_S kT}\frac{dI_{pv}}{dV_{pv}}\middle| \begin{matrix} V_{pv} = V_{mp}, \\ I_{pv} = I_{mp}\end{matrix}\right\}\end{aligned} \quad (8)$$

where I_{mp} and V_{mp} stand for the current and voltage of PV modules operated at their MPP, respectively. Moreover, when the load is disconnected, the open-circuit voltage (V_{oc}) of the thin film PV modules can be calculated by

$$\frac{I_g + N_P I_{sat}}{N_P I_{sat}} = \exp\left[\frac{qV_{oc}}{nN_S kT}\right] \quad (9)$$

By replacing the left side of Eq. (8) with the right side of Eq. (9), a characteristic equation can be obtained from Eq. (8), which represents the operation of PV modules at MPP and is expressed as

$$\begin{aligned}& \exp\left[\frac{q}{nN_S kT}\left(V_{oc} - V_{mp} - I_{mp}R_s\right)\right] \\ & = 1 + \frac{qV_{mp}}{nN_S kT} + \frac{qV_{mp}R_s}{nN_S kT}\frac{dI_{pv}}{dV_{pv}}\middle| \begin{matrix} V_{pv} = V_{mp}, \\ I_{pv} = I_{mp}\end{matrix}\end{aligned} \quad (10)$$

On the other hand, for a line-connected PV system, the effective line power P_S can be written as [35]

$$P_S = V_S \cdot I_S \cos\theta = V_S \cdot I_T \quad (11)$$

where V_S and I_S are the RMS values of the line voltage (V) and the line current (A), θ is the angle of the line current (radians), and the RMS value of the line current is $I_T = I_S \cos\theta$ (A). Considering the law of power conservation and the power conservation efficiency, the effective line power P_S should be equal to the DC power P_{pv} generated by PV modules multiplied with its conservation efficiency, that is,

$$P_S = \eta P_{pv} \quad (12)$$

where η is the power conservation efficiency of the thin film PV modules. From Eqs (4), (11), and (12), the DC current I_{pv} of the PV modules can be estimated as follows:

$$I_{pv} = \frac{P_{pv}}{V_{pv}} = \frac{P_S}{\eta V_{pv}} = \frac{V_S I_T}{\eta V_{pv}} \quad (13)$$

Thus, the characteristic equation for PV modules operated at the MPP becomes

$$\begin{aligned}& \exp\left[\frac{q}{nN_S kT}\left(V_{oc} - V_{mp} - \frac{V_S I_T}{\eta V_{mp}}R_s\right)\right] \\ & = 1 + \frac{qV_{mp}}{nN_S kT} - \frac{qR_s}{nN_S kT}\frac{V_S I_T}{\eta V_{mp}}\end{aligned} \quad (14)$$

The η can be considered as a constant in this model because η can reach up to 99% with a line connection. The open-circuit voltage V_{oc} under standard test conditions can be obtained from the datasheet for the thin film PV modules. In practical applications, the voltage V_{mp} of a thin film PV module operated at the MPP is near linearly proportional to the open-circuit voltage V_{oc} of a thin film PV module operated under different environmental conditions, that is, varying irradiation intensities and temperatures [34]. In order to directly estimate the MPP of thin film PV modules, the voltage V_{mp} at the MPP can be expressed as proportional to the open-circuit voltage V_{oc}:

$$V_{mp} = mV_{oc} \quad (15)$$

where m is defined as the ratio of V_{mp} to V_{oc}. Substituting Eq. (15) into Eq. (14), the characteristic equation becomes

$$\exp\left[\frac{q}{nN_S kT}\left(V_{oc} - mV_{oc} - \frac{V_S I_T}{\eta m V_{oc}} R_s\right)\right] \quad (16)$$

$$= 1 + \frac{qmV_{oc}}{nN_S kT} - \frac{qR_s}{nN_S kT}\frac{V_S I_T}{\eta m V_{oc}}$$

The value of m can be calculated by Eq. (16), regardless of the aforementioned parameters associated either with the semiconductor fabrication procedure or with on-line measurable values. The q, n, and k are physical constants; V_{oc}, R_s, N_S, η, and T are the experimental parameters; V_S and I_T are the measuring parameters. Subsequently, we can directly obtain the MPPs of thin film PV modules in real time from Eq. (15).

To sum up, we can directly estimate the MPP of thin film PV modules with the proposed method. From the development of the proposed method and on the basis of our experiment results, we can expect the prediction performance of the method to be robust for various series-connected and parallel-connected combinations of cells in thin film PV modules. In the characteristic equation, that is, Eq. (16), the q, n, and k are physical constants, and the characteristic parameters of thin film PV modules, such as V_{oc}, R_s, and N_S can be obtained from the data sheets for the thin film PV modules. The effective line power ($P_S = V_S I_T$) of a line-connected PV system with constant power conservation efficiency (η) can be directly measured. The ambient temperature (T) can also be measured for thin film PV modules under various operation conditions. Substituting the values of the physical constants, experimental parameters, and measured parameters into Eq. (16), we can directly obtain the m value (which is defined as the ratio of V_{mp} to V_{oc}) and then use Eq. (15) to estimate the V_{mp} at the MPP of thin film PV modules. Because our method is based on the inherent properties of semiconductor materials, it is also not affected by the fabrication procedure of the PV modules. This further guarantees that variations in the operating conditions (such irradiation and ambient temperature) that occur in practical applications will have little effect on the PV modules. The proposed method is a new and simple approach with a low calculation burden, which can be used to directly determine the MPP of thin film PV modules. The MPPT algorithm can be combined with the proposed direct-prediction method to construct the control algorithms that will accurately track the MPP of the PV modules. The proposed method shows promise to allow PV modules to achieve maximum power output in real time for practical applications of PV modules.

3. EXPERIMENTAL PROCEDURES

In this study, we develop a prediction method capable of directly estimating the MPP of the thin film PV module. The output current and voltage of thin film PV modules tend to vary with the internal resistance, illumination, and ambient temperature. The performance of the proposed method is evaluated through examining the characteristics of the MPP of thin film PV modules with respect to various irradiation intensities and ambient temperatures, and the results are discussed in detail in the next section.

Because of the limitations of experimental setups, the performance of the proposed method is evaluated with respect to various ambient temperatures and irradiation intensities. Even with varying the numbers of series-connected and parallel-connected cells, the experimental results show that the proposed method can certainly be used to directly determine the MPP of thin film PV modules from the irradiated current–voltage (I–V) characteristic curves.

We conducted the field data tests and examined the irradiation intensity-dependent and ambient temperature-dependent characteristics of thin film PV modules. In order to efficiently determine the feasibility of the method, we used various irradiation intensities and ambient temperatures. Thin film PV modules composed of six parallel-connected sub-modules, each sub-module comprised 106 series-connected Si cells, were used in the field tests. Figure 2 shows a schematic diagram of the field data tests of the characteristics of the thin film PV modules. The power supply instrument was a solar simulator (SPI-SUN SIMULATOR 4600, Spire, Bedford, MA, USA). To

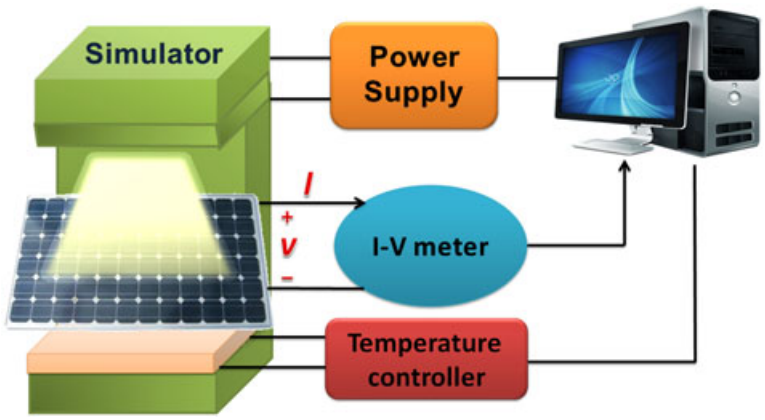

Figure 2. A schematic diagram showing the field data tests for the irradiation intensity characteristic of thin film PV modules.

DOI: 10.1002/pip

observe the characteristics of irradiation intensity dependence, a temperature control system was used that received signals from a temperature sensor, for example, a thermocouple or a resistance temperature detector, which in turn acted as input to accurately control the experimental temperature without extensive operator involvement. In addition, the temperature controller was connected to a cooling stage to maintain a stable ambient temperature. The actual temperature was compared with the desired control temperature, or set point, to provide output to a control element. Before measuring the *I–V* characteristics, the PV modules were placed stably on the cooling stage, and the ambient temperature was maintained at a specified value. The power supply, *I–V* meter, and temperature controller are also connected and controlled with a personal computer, as depicted in Figure 2.

Firstly, we measured the *I–V* characteristics of thin film PV modules with the *I–V* meter under standard test conditions, that is, an irradiation intensity of 1000 W/m^2, AM 1.5G, and an ambient temperature of 25 °C. The *I–V* characteristics of thin film PV modules were also examined under different illumination levels and ambient temperatures as supplied by the solar simulator (SPI-SUN SIMULATOR 4600, Spire). The illumination intensities during the field tests were 200, 500, 800, and 1000 W/m^2. The experiments for field tests were conducted at five temperatures, i.e., 0, 25, 50, 75, and 100 °C, respectively. The *I–V* characteristics of thin film PV modules were measured with respect to the different illumination levels and ambient temperatures. The measurement for each test condition was repeated 100 times to obtain the field test data of the PV modules. The MPP of thin film PV modules under different irradiation intensities and ambient temperatures were then determined using the proposed direct-prediction method, and this process will be discussed in detail as follows.

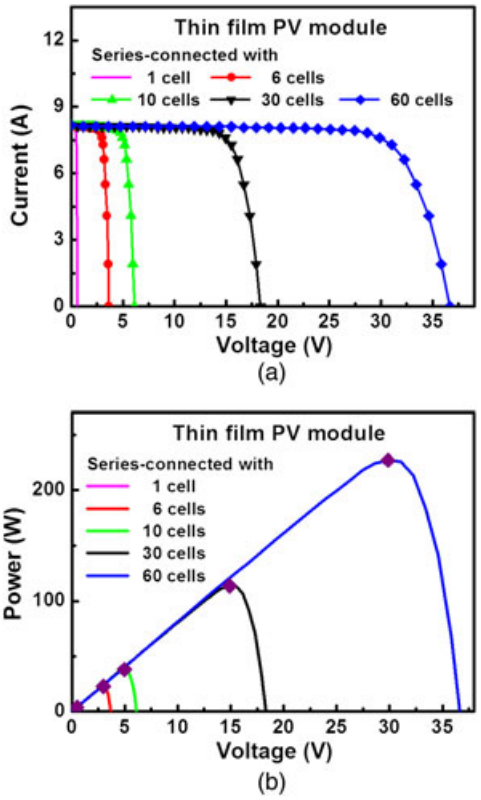

Figure 3. The (a) current–voltage and (b) power–voltage curves for thin film PV modules with different numbers of series-connected cells under an irradiation intensity of 1000 W/m^2, AM 1.5G, and an ambient temperature of 25 °C. The diamond symbols on the power–voltage curves in (b) indicate the MPPs of thin film PV modules with different series-connected numbers estimated by the direct-prediction method.

4. RESULTS AND DISCUSSION

4.1. Basic performance evaluation: the effect of the number of series-connected and parallel-connected cells

We examined the feasibility of the proposed direct-prediction method with experiments for both series-connection and parallel-connection thin film PV modules. The experimental measurements were carried out using the standard test conditions (an irradiation intensity of 1000 W/m^2, AM 1.5G, and an ambient temperature of 25 °C).

Figure 3(a and b) show the current–voltage (*I–V*) and power–voltage (*P–V*) curves for thin film PV modules with different numbers of series-connected cells (N_S). The number (N_S) of cells in the thin film PV series-connected modules is 1, 6, 10, 30, or 60 cells. For the series-connected PV modules, the output current remains unchanged, but the output voltage increases with increasing series-connected cell numbers. Therefore, it is obvious that the output voltage is proportional to N_S and the value of the output current is irrelevant to N_S, as shown in Figure 3(a). It can be seen in Figure 3(b) that the output power of thin film PV modules also increases with increasing numbers of series-connected cells. The diamond symbols on the power–voltage curves in Figure 3(b) indicate the MPPs of thin film PV modules for different series-connected numbers as estimated by the direct-prediction method, that is, through Eqs (15) and (16). It is also found that the values of V_{mp} will rise with increasing series-connected numbers. Clearly, the proposed method can certainly be used to directly determine the MPPs of thin film PV modules from the irradiated current–voltage (*I–V*) characteristic curves, even for various numbers of series-connected cells.

To clarify the relationship between the MPP and different parallel connections, we examine the *I–V* and *P–V* curves for thin film PV modules with different numbers (N_P) of parallel-connected cells (1, 2, 6, 12, or 20 cells) as shown in Figure 4(a and b). Note that parallel connection of the cells increases the output current. It is worth mentioning that the values of the current rise with increasing numbers of parallel-connected cells, as shown in Figure 4(a). This phenomenon is different from that shown in Figure 3(a). Moreover, the output power of thin film PV modules also increases with increasing series-connected

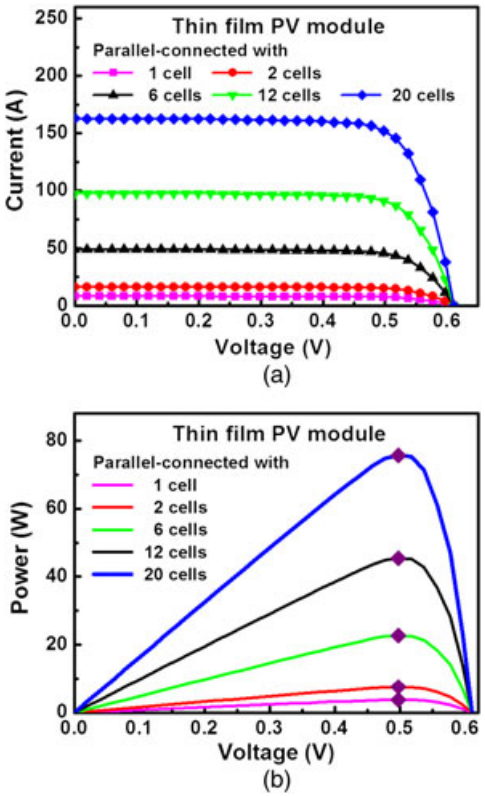

Figure 4. The (a) current–voltage and (b) power–voltage curves for thin film PV modules with different numbers of parallel-connected cells under an irradiation intensity of 1000 W/m^2, AM 1.5G, and an ambient temperature of 25 °C. The diamond symbols on the power–voltage curves in (b) indicate the MPPs of thin film PV modules with different parallel-connected numbers estimated by the direct-prediction method.

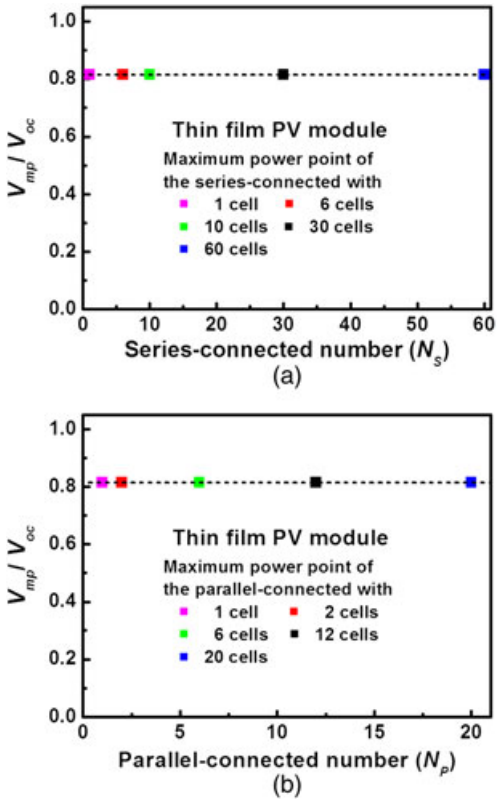

Figure 5. The characteristic ratios of V_{mp}/V_{oc} of thin film PV modules with (a) different parallel-connected cell numbers (N_S) and (b) different parallel-connected cell numbers (N_P) under an irradiation intensity of 1000 W/m^2, AM 1.5G, and an ambient temperature of 25 °C.

numbers. The direct-prediction method is also used to examine the MPPs of the tested thin film PV modules with different parallel-connected cell numbers. The results are indicated by the diamond symbols on the power–voltage curves in Figure 4(b). The experimental results show that the values of V_{mp} for the MPPs of thin film PV modules remain unchanged and insensitive to various parallel-connected numbers (N_P), which is in agreement with the theoretical implications derived from Eq. (16).

The ratios of V_{mp}/V_{oc} for the thin film PV modules also vary with different N_S and N_P connections as plotted in Figure 5(a and b). The results are consistent with the proposed theoretical model. The values of m (which is defined as the ratio of V_{mp} to V_{oc}) are invariant under various numbers of series-connected (N_S) and parallel-connected (N_P) cells, remaining almost constant (close to 0.814) when N_S and N_P increase. These experiments confirm that the method presented here is accurate and simple to calculate. Furthermore, the experimental results shown in Figure 6(a and b) further demonstrate that the parallel-connected number (N_P) has only a slight impact on the characteristic of the thin film PV modules, or the determination of the MPPs of thin film PV modules. From Figure 6(a and b), we can see that either V_{mp} or V_{oc} has a proportional relationship to N_S; however, a constant relationship to N_P is revealed. The interrelationship between V_{mp} and V_{oc} presents an incremental phenomenon in the cases where N_S varies and an almost invariant property in the cases where N_P varies. Therefore, our method is an effective way to determine the MPP of thin film PV modules from a single irradiated I–V characteristic curve. The effect of series-connected cell numbers (N_S) can also be taken into consideration in practical applications.

Our previous theoretical method [34] can also be used to further examine the relationship between the short-circuit current I_{sc} and the current I_{mp} at the MPPs for the thin film PV modules by looking at the characteristic ratios of I_{mp}/I_{sc} of thin film PV modules with respect to different N_S and N_P. Figure 7(a and b) shows the characteristic ratios of I_{mp}/I_{sc} of thin film PV modules with different N_S and N_P connections under the standard test conditions. The short-circuit current I_{sc} and the current I_{mp} at the MPPs of thin film PV modules vary simultaneously with the numbers of N_S and N_P, but the characteristic ratios of I_{mp}/I_{sc} of thin film PV modules remain unchanged with this variation. A comparison of the calculated results and the experimental results in Figure 7(a and b) shows that both are pretty similar.

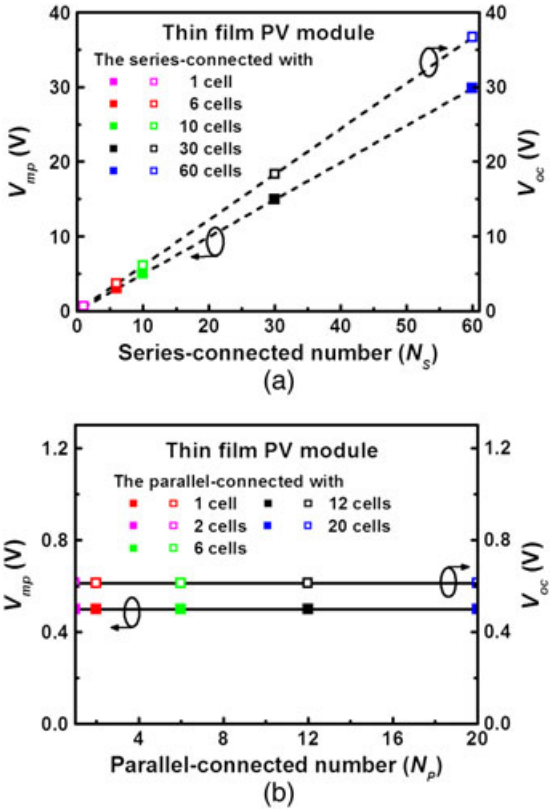

Figure 6. The (a) V_{mp}–N_S–V_{oc} and (b) V_{mp}–N_P–V_{oc} characteristics of thin film PV modules for different numbers of series-connected (N_S) and parallel-connected (N_P) cells under an ambient temperature of 25 °C.

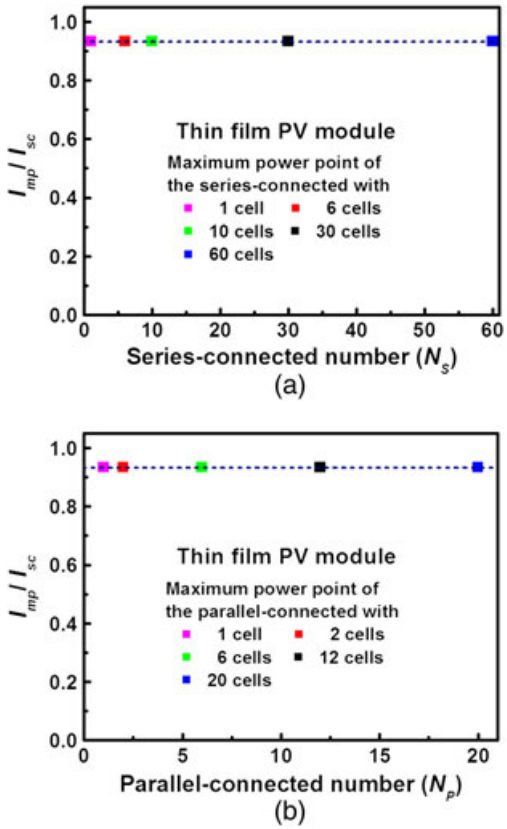

Figure 7. The characteristic ratios of I_{mp}/I_{sc} of thin film PV modules with (a) different numbers of parallel-connected cells (N_S) and (b) different parallel-connected cells (N_P) under an irradiation intensity of 1000 W/m^2, AM 1.5G, and an ambient temperature of 25 °C.

Figure 8(a and b) can be used to uncover the relationship between currents (I_{mp} and I_{sc}) and cell numbers (N_S and N_P). Figure 8(a) shows that I_{mp} or I_{sc} remains constant while N_S is changed. However, Figure 8(b) reveals that there exists a proportional relationship of I_{mp} or I_{sc} to N_P. The interrelationship between I_{mp} and I_{sc} indicates an almost invariant property in the cases of N_S variation and an incremental phenomenon in the case of N_P variation. All of the aforementioned phenomena are opposite to the voltage ones (Figure 6). These experimental results verify that the current at the MPP of the thin film PV module can also be accurately estimated using our previous theoretical method [34]. Moreover, it is confirmed that there is a proportional relationship between the short-circuit current I_{sc} and the current I_{mp} of the MPP, which is almost constant and equal to 0.93. Our approach is more accurate than the empirically current ratio of I_{mp}/I_{sc} reported in [22], even when the series-connected cell numbers and parallel-connected cell numbers change.

4.2. Performance evaluation for various irradiation intensities and ambient temperatures

Figures 9 and 10 show the current–voltage (I–V) and power–voltage (P–V) curves of the tested thin film PV modules under different irradiation intensities and an ambient temperature of 25 °C. For the standard test, the open-circuit voltage V_{oc} and short-circuit current I_{sc} of the tested thin film PV modules are 97 V and 1.62 A, respectively. As mentioned previously, the adopted power conservation efficiency η for the parallel-connected PV power conditioning system when line connection is set as $\eta = 98\%$. The ideality factor n of the thin film PV modules in this study is set to be $n = 1.3$. The factor of n is the expected value between the diffusion ("1") and the generation recombination mechanisms ("2") [33]. Most importantly, the effects of various irradiation intensities on the I–V curve of the thin film PV modules are the main issues investigated in detail.

In this study, we used four different irradiation intensities of 200, 500, 800, and 1000 W/m^2 in our examination of the feasibility of applying the proposed direct-prediction method to determine the MPPs of thin film PV modules under various irradiation conditions. The irradiation intensity dependence of the V_{oc}, V_{mp}, and V_{mp}/V_{oc} for the thin film PV modules at a temperature of 25 °C is summarized in Table I. From Table I, it can be seen that the values of the open-circuit voltage V_{oc} and the voltage V_{mp} at the MPP of the thin film PV modules vary slightly with the increased irradiation intensity.

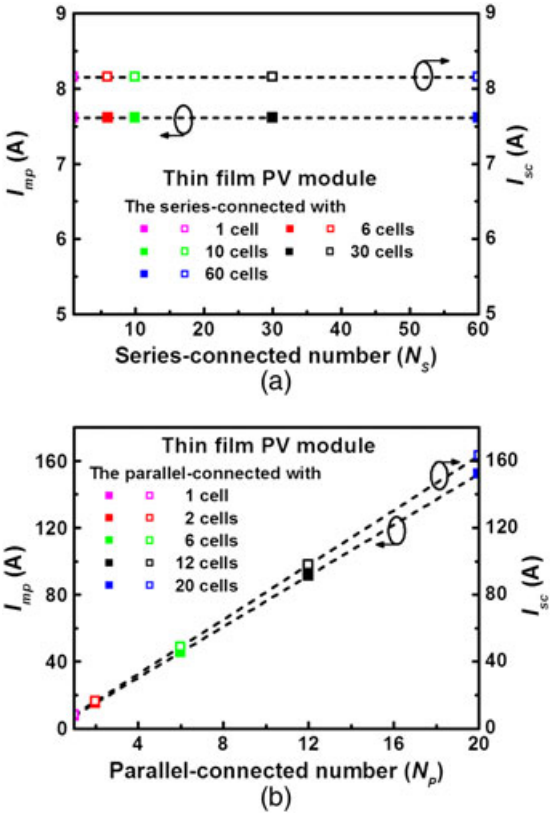

Figure 8. The (a) I_{mp}–N_S–I_{sc} and (b) I_{mp}–N_P–I_{sc} characteristics of thin film PV modules for different numbers of series-connected (N_S) and parallel-connected (N_P) cells under an ambient temperature of 25 °C.

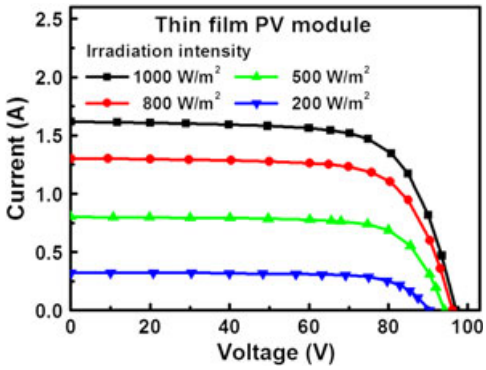

Figure 9. The current–voltage curves of thin film PV modules under different irradiation intensities and an ambient temperature of 25 °C.

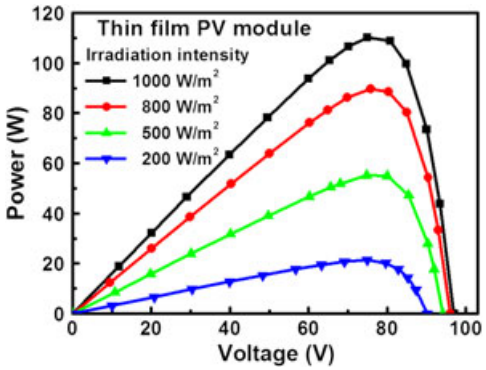

Figure 10. The power–voltage curves of thin film PV modules under different irradiation intensities and an ambient temperature of 25 °C.

Next, we want to investigate the prediction performance of the proposed direct-prediction method. To this end, two prediction performance indices are defined: (1) prediction error in V_{mp}: $|\Delta V_{mp}| = |V_{mp(\text{direct-prediction method})} - V_{mp(\text{Experimental results})}|$; and (2) percentage prediction error in V_{mp}/V_{oc}: $|V_{mp}/V_{oc}|\ (\%) = |[(V_{mp}/V_{oc(\text{direct-prediction method})} - V_{mp}/V_{oc(\text{Experimental results})})/(V_{mp}/V_{oc(\text{Experimental results})})] \times 100\%|$. The two prediction performance indices for thin film PV modules obtained by the direct-prediction method, by using the data in Table I, are summarized in Table II. The average values of the prediction error $|\Delta V_{mp}|$ and the percentage prediction error $|V_{mp}/V_{oc}|$ (%) for the actual and estimated maximum power voltages of the thin film PV modules are 1.1192 V and 1.68%, respectively. This confirms that the voltage V_{mp} at the MPP of the thin film PV module can be simply and accurately estimated by using the direct-prediction method.

Figure 11 shows the characteristic ratio of V_{mp}/V_{oc} and I_{mp}/I_{sc} for the thin film PV module estimated by the direct-prediction method under different irradiation intensities and an ambient temperature of 25 °C. After careful inspection of Figure 11, we find that the ratios of V_{mp}/V_{oc} remain almost constant, close to 0.78. Furthermore, from the values of V_{mp} and V_{oc}, we can also directly estimate the ratio of I_{mp} and I_{sc} at the MPPs of the thin film PV modules through the theoretical method [34]. Figure 11 also shows the irradiation intensity dependence of I_{mp}/I_{sc} ratio for the thin film PV modules. In contrast to the slight decrease in the ratio of V_{mp}/V_{oc}, the experimental results show that I_{mp}/I_{sc} remains almost constant when the irradiation intensity increases. These facts are important for finding the operation characteristics of thin film PV modules.

Figure 12 depicts the relationship between the short-circuit current I_{sc} and the current I_{mp} at the MPP for the thin film PV under different irradiation intensities and an ambient temperature of 25 °C. The linearly proportional relationship between the short-circuit current I_{sc} and the current I_{mp} of the MPP remains almost constant and is equal to 0.92. This result is more accurate than the empirically current proportion of I_{mp}/I_{sc} reported in [22], even if the irradiation intensity changes.

Table III lists the measurement data for I_{sc}, I_{mp}, and I_{mp}/I_{sc} of the thin film PV modules and their corresponding estimation results obtained using the direct-prediction method. The measurement experiments were conducted with four different irradiation levels while maintaining the solar panels at a constant temperature. From Table III, it can be clearly seen that the current I_{mp} of the MPP is proportional

Table I. The measured data of V_{oc}, V_{mp}, and V_{mp}/V_{oc} for thin film PV modules and the corresponding estimation results obtained by using the direct-prediction method under different irradiation intensities and an ambient temperature of 25 °C.

Irradiation intensity (W/m^2)	Experimental results			Direct-prediction method	
	V_{oc} (V)	V_{mp} (V)	V_{mp}/V_{oc}	V_{mp} (V)	V_{mp}/V_{oc}*
1000	97.0061	74.9462	0.7726	75.2282	0.7755
800	96.0897	75.7685	0.7885	74.7578	0.7780
500	94.1332	74.7389	0.7940	74.6006	0.7925
200	90.2550	74.9565	0.8305	71.3466	0.7905

*The values of the open-circuit voltage (V_{oc}) used are the same as the experimental ones.

Table II. The prediction performance indices expressed as prediction error ($|\Delta V_{mp}|$) and percentage of prediction error ($|V_{mp}/V_{oc}|$) for thin film PV modules obtained by using the direct-prediction method under different irradiation intensities and an ambient temperature of 25 °C.

Irradiation intensity (W/m^2)	Prediction performance indices	
	Prediction error $|\Delta V_{mp}|$ (V)	Percentages of prediction error $|V_{mp}/V_{oc}|$ (%)
1000	0.2820	0.38
800	1.0107	1.33
500	0.1383	0.19
200	3.6099	4.82

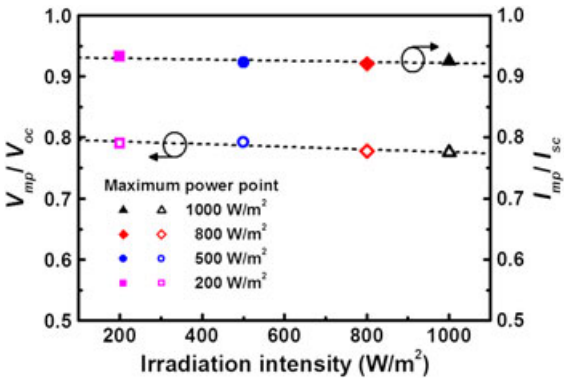

Figure 11. The characteristic ratios of V_{mp}/V_{oc} and I_{mp}/I_{sc} for thin film PV modules estimated by the direct-prediction method under different irradiation intensities and an ambient temperature of 25 °C.

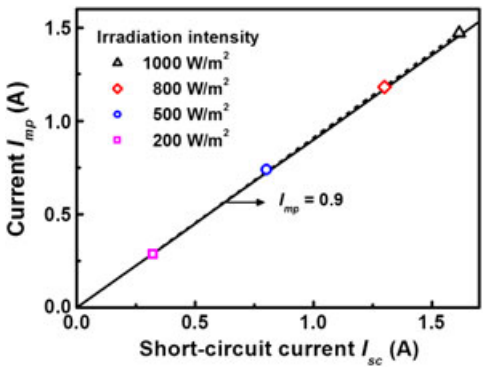

Figure 12. The relationship between the short-circuit current I_{sc} and the current I_{mp} at the MPPs for thin film PV modules estimated by the direct-prediction method under different irradiation intensities and an ambient temperature of 25 °C.

to the irradiation intensity. Furthermore, the values of the short-circuit current I_{sc}, the current I_{mp} of the MPP, and the ratio of I_{mp}/I_{sc} are all correlated with the irradiation intensity level. More importantly, an examination of Table III indicates that the ratio of I_{mp}/I_{sc} remains almost constant and close to 0.925. Table IV summarizes the prediction performance indices for thin film PV modules, including prediction error ($|\Delta I_{mp}|$) and percentage of prediction error ($|I_{mp}/I_{sc}|$) obtained with the direct-prediction method. These two parameters are defined as follows: (1) prediction error in I_{mp}: $|\Delta I_{mp}| = |I_{mp(\text{direct-prediction method})} - I_{mp(\text{Experimental results})}|$; and (2) percentage prediction error in I_{mp}/I_{sc}: $|I_{mp}/I_{sc}|$ (%) = $|[(I_{mp}/I_{sc(\text{direct-prediction method})} - I_{mp}/I_{sc(\text{Experimental results})})/(I_{mp}/I_{sc(\text{Experimental results})})] \times 100\%|$. As can be seen in Table IV, the average values of the prediction error $|\Delta I_{mp}|$ and the average prediction error $|I_{mp}/I_{sc}|$ (%) are 0.025 A and 2.06%, respectively. By using the proposed direct-prediction method, very accurate estimations of I_{mp} and I_{mp}/I_{sc} can be obtained.

Temperature variation always seriously affects the performances of thin film PV modules. Therefore, the temperature dependence of the proposed prediction method needs to be carefully examined. The current–voltage (I–V) and power–voltage (P–V) curves obtained for the thin film PV modules tested under different ambient temperatures with an irradiation intensity of 1000 W/m^2

Table III. The measured data I_{sc}, I_{mp}, and I_{mp}/I_{sc} for thin film PV modules and the corresponding estimation results obtained by using the direct-prediction method under different irradiation intensities and an ambient temperature of 25 °C.

Irradiation intensity (W/m^2)	Experimental results			Direct-prediction method	
	I_{sc} (A)	I_{mp} (A)	I_{mp}/I_{sc}	I_{mp} (A)	I_{mp}/I_{sc}*
1000	1.6159	1.4705	0.9100	1.4949	0.9251
800	1.3023	1.1833	0.9086	1.1993	0.9209
500	0.8013	0.7382	0.9212	0.7395	0.9229
200	0.3218	0.2856	0.8877	0.3001	0.9326

*The values of the short-circuit current (I_{sc}) used are the same as the experimental ones.

Table IV. The prediction performance indices expressed as prediction error ($|\Delta I_{mp}|$) and percentage of prediction error ($|I_{mp}/I_{sc}|$) for thin film PV modules obtained by using the direct-prediction method under different irradiation intensities and an ambient temperature of 25 °C.

Irradiation intensity (W/m^2)	Prediction performance indices	
	Prediction error $|\Delta I_{mp}|$ (A)	Percentages of prediction error $|I_{mp}/I_{sc}|$ (%)
1000	0.0244	1.66
800	0.0405	1.35
500	0.0165	0.19
200	0.0206	5.06

are shown in Figures 13 and 14, respectively. In these tests, the material parameters, the ideality factor n and the power conservation efficiency η, are set the same as mentioned earlier, that is, 1.3 and 98%, respectively. The experimental results show that the performances of the thin film PV modules are affected by the temperature, with the voltage of the thin film PV module decreasing as the temperature climbs. From Figure 13, it can be observed that the change in temperature mainly influences the PV output voltage. As the device temperature goes up, V_{oc} will rapidly decline because of the exponential dependence of the saturation current I_{sat} on temperature while I_{sc} slightly increases [33].

In this experiment, we used five different ambient temperatures of 0, 25, 50, 75, and 100 °C and further examined the feasibility of the proposed direct-prediction method when applied to determine the MPPs of thin film PV modules under different ambient temperatures. The results of the ambient temperature dependence of the V_{oc}, V_{mp}, and V_{mp}/V_{oc} for thin film PV modules at an irradiation intensity of 1000 W/m^2 are summarized in Table V. It can be seen that the values of the open-circuit voltage V_{oc} and the voltage V_{mp} at the MPP of the thin film PV modules decrease with an increase in the ambient temperature. The prediction performance of the proposed direct-prediction method is similarly investigated. The two prediction performance indices for thin film PV modules generated by the direct-prediction method based on the data of Table V are summarized in Table VI. Both prediction performance indices are defined as before. It can be seen in Table VI that the average values of the prediction error $|\Delta V_{mp}|$ and the percentage prediction error $|V_{mp}/V_{oc}|$ (%) for the actual and estimated maximum power voltages of the thin film PV modules are 1.0988 V and 1.65%, respectively. These results confirm that the voltage V_{mp} at

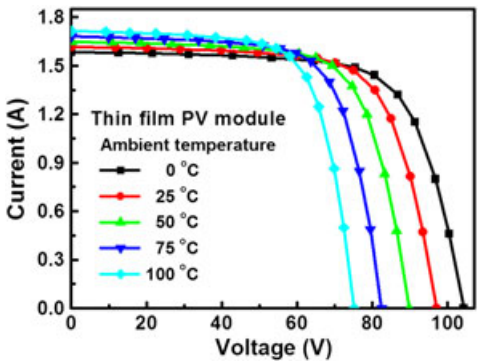

Figure 13. The current–voltage curves of thin film PV modules under different ambient temperatures and an irradiation intensity of 1000 W/m^2.

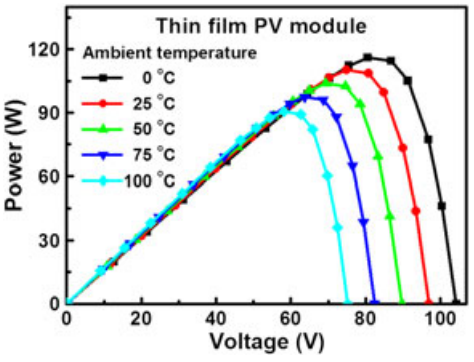

Figure 14. The power–voltage curves of thin film PV modules under different ambient temperatures and an irradiation intensity of 1000 W/m^2.

Table V. The measured data V_{oc}, V_{mp}, and V_{mp}/V_{oc} for thin film PV modules and the corresponding estimation results obtained by using the direct-prediction method under different ambient temperatures and an irradiation intensity of 1000 W/m^2.

Ambient temperature (°C)	Experimental results			Direct-prediction method	
	V_{oc} (V)	V_{mp} (V)	V_{mp}/V_{oc}	V_{mp} (V)	V_{mp}/V_{oc}*
0	104.2816	80.5669	0.7720	81.4439	0.7810
25	97.0061	74.9459	0.7720	74.6947	0.7700
50	89.7306	69.3250	0.7720	68.3299	0.7615
75	82.4552	63.7041	0.7720	62.2949	0.7555
100	75.1797	58.0831	0.7720	56.1217	0.7465

*The values of the open-circuit voltage (V_{oc}) used are the same as the experimental ones.

Table VI. The prediction performance indices expressed as prediction error ($|\Delta V_{mp}|$) and percentage of prediction error ($|V_{mp}/V_{oc}|$) for thin film PV modules obtained by using the direct-prediction method under different ambient temperatures and an irradiation intensity of 1000 W/m^2.

Ambient temperature (°C)	Prediction performance indices	
	Prediction error $|\Delta V_{mp}|$ (V)	Percentages of prediction error $|V_{mp}/V_{oc}|$ (%)
0	0.8770	1.17
25	0.2512	0.26
50	0.9951	1.36
75	1.4091	2.14
100	1.9615	3.30

the MPP of the thin film PV module can be simply and accurately estimated using the direct-prediction method.

Figure 15 shows the characteristic ratio of V_{mp}/V_{oc} and I_{mp}/I_{sc} for thin film PV modules estimated by the direct-prediction method under different ambient temperatures and an irradiation intensity of 1000 W/m^2. The solid lines in Figure 15 indicate the experimental results; the dashed lines represent the results obtained by direct-prediction method. Both ratios of V_{mp}/V_{oc} and I_{mp}/I_{sc} clearly remain almost constant. In addition, after direct estimation, the V_{mp}/V_{oc} results (represented by the dashed line) decreased slightly with the rise in the ambient temperature. In contrast to the slight decrease in the ratio of V_{mp}/V_{oc}, the I_{mp}/I_{sc} ratio showed a tendency to increase when the ambient temperature was raised. These facts are important for finding the operation characteristics of thin film PV modules. To clarify this, we plotted the curves showing the variation of I_{mp} and I_{sc} with temperature in Figure 16. It can be easily seen that both currents rise with increasing ambient temperature. The I_{mp} and I_{sc} curves appear like two parallel lines; see the determination of the phenomenon in Figure 15.

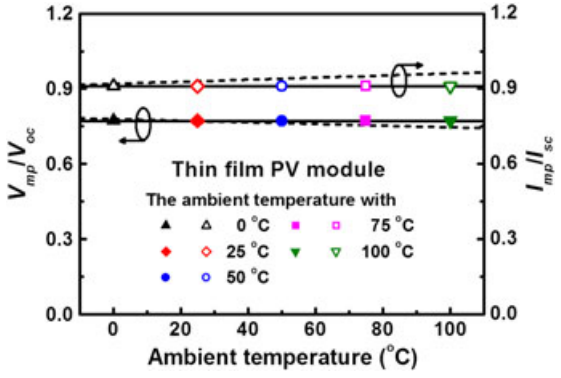

Figure 15. The characteristic ratios of V_{mp}/V_{oc} and I_{mp}/I_{sc} for thin film PV modules estimated by the direct-prediction method under different ambient temperatures and an irradiation intensity of 1000 W/m^2. The solid lines indicate the experimental results, and the dashed lines indicate the results obtained by the direct-prediction method.

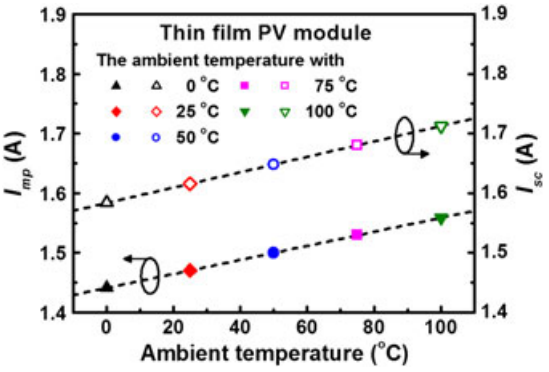

Figure 16. The relationship between the short-circuit current I_{sc} and the current I_{mp} at the MPPs for thin film PV modules estimated by the direct-prediction method under different ambient temperatures and an irradiation intensity of 1000 W/m^2.

Table VII. The measured data I_{sc}, I_{mp}, and I_{mp}/I_{sc} for thin film PV modules and the corresponding estimation results obtained by using the direct-prediction method under different ambient temperatures and an irradiation intensity of 1000 W/m^2.

Ambient temperature (°C)	Experimental results			Direct-prediction method	
	I_{sc} (A)	I_{mp} (A)	I_{mp}/I_{sc}	I_{mp} (A)	I_{mp}/I_{sc}*
0	1.5835	1.4411	0.9100	1.4546	0.9186
25	1.6159	1.4705	0.9100	1.5055	0.9317
50	1.6482	1.4999	0.9100	1.5528	0.9421
75	1.6805	1.5293	0.9100	1.5958	0.9496
100	1.7128	1.5587	0.9100	1.6461	0.9611

*The values of the short-circuit current (I_{sc}) used are the same as the experimental ones.

Table VIII. The prediction performance indices expressed as prediction error ($|\triangle I_{mp}|$) and percentage of prediction error ($|I_{mp}/I_{sc}|$) for thin film PV modules obtained by using the direct-prediction method with different ambient temperatures and an irradiation intensity of 1000 W/m^2.

Ambient temperature (°C)	Prediction performance indices	
	Prediction error $|\triangle I_{mp}|$ (A)	Percentages of prediction error $|I_{mp}/I_{sc}|$ (%)
0	0.0136	0.94
25	0.0351	2.38
50	0.0529	3.53
75	0.0665	4.35
100	0.0874	5.61

The measurement data for I_{sc}, I_{mp}, and I_{mp}/I_{sc} for the tested thin film PV modules and their corresponding estimation results obtained using the direct-prediction method are shown in Table VII. The values of the short-circuit current I_{sc}, the current I_{mp} of the MPP, and the ratio of I_{mp}/I_{sc} are all correlated with the variation in the ambient temperature. From Table VII, it can also be found that the ratio of I_{mp}/I_{sc} remains almost constant, close to 0.91.

Table VIII summarizes the prediction performance indices for thin film PV modules, that is, prediction error ($|\Delta I_{mp}|$) and percentages of prediction error ($|I_{mp}/I_{sc}|$), estimated by the proposed direct-prediction method to examine its feasibility. The parameters are defined as mentioned earlier. From Table VIII, we can find that the average values of the prediction error $|\Delta I_{mp}|$ and prediction error $|I_{mp}/I_{sc}|$ (%) are 0.05 A and 3.36%, respectively. With these facts, the current I_{mp} at the MPP of the thin film PV module can be simply and accurately estimated using the direct-prediction method. Irradiation intensity and ambient temperature directly affect the performance of the thin film PV modules that convert solar energy into DC electricity and continuously provide a DC forward current. On the basis of the data summarized in Tables VI and VIII, with an increase in the ambient temperature, it was found that the temperature difference in the interior of the PV modules gradually went up because of the packaging thermal structure and material properties. The electrical characteristics of PV modules were slightly affected by the significant self-heating effect and the thermal accumulation of the PV modules, causing greater variations in the estimation of the current and voltage (I_{mp} and V_{mp}) of PV modules operated at the MPP. Therefore, the percentage of prediction error ($|V_{mp}/V_{oc}|$ and $|I_{mp}/I_{sc}|$) of thin film PV modules under a higher ambient temperature is higher than that under a lower ambient temperature. With these findings, we can conclude that the proposed direct-prediction method can be used to obtain pretty accurate estimations of V_{mp}, I_{mp}, V_{mp}/V_{oc}, and I_{mp}/I_{sc} under different irradiation intensities or ambient temperatures.

The experimental results and theoretical estimations demonstrate that we can directly and accurately estimate the values of the characteristic index, m, for thin film PV modules composed of different numbers of series-connected and parallel-connected cells under different irradiation intensities and temperatures. This fact guarantees that the proposed direct-prediction prediction method for the MPPs of thin film PV modules can be used to develop control rules for MPPT control for PV arrays/systems.

5. CONCLUSIONS

In this study, we propose a new, simple, accurate method with a low calculation burden for the estimation of the MPP of thin film PV modules. This efficient and direct-prediction method is developed on the basis of the p–n junction recombination mechanism. The MPP of thin film PV modules with any number of series-connected and parallel-connected cells can be simply estimated even under different irradiation intensities and temperatures. The proposed method can be used to directly determine the MPP of thin film PV modules with the changes of the irradiation intensity

and temperature. The average values of the percentage prediction error $|V_{mp}/V_{oc}|$ (%) for the actual and estimated maximum power voltages of thin film PV modules are 1.68% and 1.65% (under various irradiation intensities and temperatures). These results confirm that the location of the MPP for the thin film PV module can be simply and accurately estimated using the direct-prediction method even with changes in the irradiation intensity and temperature. The evolution of the characteristic ratios V_{mp}/V_{oc} and I_{mp}/I_{sc} can be considered as a function of the irradiation intensity and temperature, and our values are found to be in good agreement with the theoretical predictions. With the direct-prediction prediction method, we can simply find the value of m (which is defined as the ratio of V_{mp} to V_{oc}) and track the MPP of the PV system with an MPPT control model in real time.

ACKNOWLEDGEMENTS

This work was financially supported in part by the National Science Council, the President of National Taiwan University, and the Council of Agriculture of the Executive Yuan, Taiwan, under the grants NSC 100-2218-E-002-005, NSC 100-2218-E-002-006, NSC 100-3113-E-002-005, NSC 100-3113-P-002-012, NSC 101-3113-E-002-005, NSC 101-ET-E-002-012-ET, 10R70606-4, 101AS-7.1.2-BQ-B1, and 101AS-7.1.2-BQ-B2. The authors are deeply grateful to Mrs. Debbie Nester for her great help in English editing. We are also grateful to the Editor and the anonymous referees for their invaluable suggestions to improve the paper.

REFERENCES

1. Hartmann D, Kaltschmitt M. Electricity generation from solid biomass via co-combustion with coal: energy and emission balances from a German case study. *Biomass and Bioenergy* 1999; **16**(6): 397–406.
2. Loitera JM, Norberg-Bohm V. Technology policy and renewable energy: public roles in the development of new energy technologies. *Energy Policy* 1999; **27**(2): 85–97.
3. Kaldellis JK, Kondili E, Filios A. Sizing a hybrid wind-diesel stand-alone system on the basis of minimum long-term electricity production cost. *Applied Energy* 2006; **83**(12): 1384–1403.
4. Fragaki A, Markvart T. Stand-alone PV system design: results using a new sizing approach. *Renewable Energy* 2008; **33**(1): 162–167.
5. Benghanem M, Mellit A. Radial basis function network-based prediction of global solar radiation data: application for sizing of a stand-alone photovoltaic system at Al-Madinah, Saudi Arabia. *Energy* 2010; **35**(9): 3751–3762.
6. Díaz P, Arias CA, Gomez-Gonzalez M, Sandoval D, Lobato R. Solar home system electrification in dispersed rural areas: a 10-year experience in Jujuy, Argentina. *Progress in Photovoltaics: Research and Applications* 2011. DOI: 10.1002/pip.1181
7. Muñoz J, Martínez-Moreno F, Lorenzo E. On-site characterisation and energy efficiency of grid-connected PV inverters. *Progress in Photovoltaics: Research and Applications* 2011; **19**(2): 192–201.
8. Marcos J, Marroyo L, Lorenzo E, Alvira D, Izco E. Power output fluctuations in large scale PV plants: one year observations with one second resolution and a derived analytic model. *Progress in Photovoltaics: Research and Applications* 2011; **19**(2): 218–227.
9. Curtright E, Apt J. The character of power output from utility-scale photovoltaic systems. *Progress in Photovoltaic: Research and Applications* 2008; **16**(3): 241–247.
10. Arribas L, Cano L, Cruz I, Mata M, Llobet E. PV–wind hybrid system performance: a new approach and a case study. *Renewable Energy* 2010; **35**(1): 128–137.
11. Kaabeche A, Belhamel M, Ibtiouen R. Sizing optimization of grid-independent hybrid photovoltaic/wind power generation system. *Energy* 2011; **36**(2): 1214–1222.
12. Dali M, Belhadj J, Roboam X. Hybrid solar–wind system with battery storage operating in grid-connected and standalone mode: control and energy management – experimental investigation. *Energy* 2010; **35**(6): 2587–2595.
13. Voivontas D, Assimacopoulos D, Mourelatos A, Corominas J. Evaluation of renewable energy potential using a GIS decision support system. *Renewable Energy* 1998; **13**(3): 333–344.
14. Nema P, Nema RK, Rangnekar S. Minimization of green house gases emission by using hybrid energy system for telephony base station site application. *Renewable and Sustainable Energy Reviews* 2010; **14**(6): 1635–1639.
15. Katti PK, Khedkar MK. Alternative energy facilities based on site matching and generation unit sizing for remote area power supply. *Renewable Energy* 2007; **32**(8): 1346–1366.
16. Pillai IR, Banerjee R. Renewable energy in India: status and potential. *Energy* 2009; **34**(8): 970–980.
17. Swanson RM. A vision for crystalline silicon photovoltaics. *Progress in Photovoltaic: Research and Applications* 2006; **14**(5): 443–453.
18. Shah A, Torres P, Tscharner R, Wyrsch N, Keppner H. Photovoltaic technology: the case for thin-film solar cells. *Science* 1999; **285**(5428): 692–698.
19. Chao CH, Chan CH, Wu FC, Huang JJ, Lien SY, Weng KW, Cheng HL. Efficient hybrid organic/

inorganic photovoltaic cells utilizing n-type pentacene and intrinsic/p-type hydrogenated amorphous silicon. *Solar Energy Materials and Solar Cells* 2011; **95**(8): 2407–2411.
20. Mutoh N, Ohno M, Inoue T. A method for MPPT control while searching for parameters corresponding to weather conditions for PV generation systems. *IEEE Transactions on Industrial Electronics* 2006; **53**(4): 1055–1065.
21. Liu F, Duan S, Liu F, Liu B, Kang Y. A variable step size INC MPPT method for PV systems. *IEEE Transactions on Industrial Electronics* 2008; **55**(7): 2622–2628.
22. Sullivan CR, Powers MJ. A high-efficiency maximum power point tracker for photovoltaic arrays in a solar-powered race vehicle. Proceeding of the 24th IEEE Power Electronics Specialists Conference (PESC'93), Seattle, U.S.A., 1993; 574–580.
23. Gow JA, Manning CD. Controller arrangement for boost converter systems sourced, from solar photovoltaic arrays or other maximum power sources. *IEE Proceedings–Electric Power Applications* 2000; **147**(1): 15–20.
24. Enslin JHR, Wolf MS, Snyman DB, Sweigers W. Integrated photovoltaic maximum power point tracking converter. *IEEE Transactions on Industrial Electronics* 1997; **44**(6): 769–773.
25. Wasynzczuk O. Dynamic behavior of a class of photovoltaic power systems. *IEEE Transactions on Power Systems* 1983; **PAS-102**(1): 3031–3037.
26. Hussein KH, Muta I, Hoshino T, Osakada M. Maximum photovoltaic power tracking: an algorithm for rapidly changing atmosphere conditions. *IEE Proceedings–Generation, Transmission and Distribution* 1995; **142**(1): 59–64.
27. Ammasai Gounden N, Peter SA, Nallandula H, Krithiga S. Fuzzy logic controller with MPPT using line-commutated inverter for three-phase grid-connected photovoltaic systems. *Renewable Energy* 2009; **34**(3): 909–915.
28. Chim CS, Neelakantan P, Yoong HP, Teo KTK. Fuzzy logic based MPPT for photovoltaic modules influenced by solar irradiation and cell temperature. Proceeding of 2011 UkSim 13th International Conference on Computer Modelling and Simulation (UKSim), Cambridge, UK, 2011; 376–381.
29. Xiao W, Dunford WG. A modified adaptive hill climbing MPPT method for photovoltaic power systems. Proceeding of the 35th IEEE Power Electronics Specialists Conference (PESC'04), Aachen, Germany, 2004; 1957–1963.
30. Paraskevadaki E, Papathanassiou S. Estimation of PV array power losses due to partial shading. Proceeding of the 25th European Photovoltaic Solar Energy Conference and Exhibition, Valencia, Spain, 2010; 4560–4564.
31. Thongpron J, Kirtikara K, Jivacate C. A method for the determination of dynamic resistance of photovoltaic modules under illumination, *Solar Energy Material and Solar Cells* 2006; **90**(18–19): 3078–3084.
32. Wang JC, Shieh JC, Su YL, Kuo KC, Chang YW, Liang YT, Chou JJ, Liao KC, Jiang JA. A novel method for the determination of dynamic resistance for photovoltaic modules. *Energy* 2011; **36**(10): 5968–5974.
33. Sze SM. Physics of Semiconductor Devices, 2nd edn. Wiley: New York, 1981.
34. Wang JC, Su YL, Shieh JC, Jiang JA. High-accuracy maximum power point for photovoltaic arrays. *Solar Energy Material and Solar Cells* 2011; **95**(3): 843–851.
35. Kwon JM, Nam KH, Kwon BH. Photovoltaic power conditioning system with line connection. *IEEE Transactions on Industrial Electronics* 2006; **53**(4): 1048–1054.